energies

MDPI

Article

Investigation of Energy Consumption via an Equivalent Thermal Resistance-Capacitance Model for a Northern Rural Residence

Ligai Kang [1,2], Hao Li [3,4], Zhichao Wang [3,4,*], Jinzhu Wang [1,2], Dongxiang Sun [1,2] and Yang Yang [1,2]

1 School of Civil Engineering, Hebei University of Science and Technology, Shijiazhuang 050018, China; ligaikang@hebust.edu.cn (L.K.); jinzhuwang0111@163.com (J.W.); sundongxiang1224@163.com (D.S.); yangyang68998@hebust.edu.com (Y.Y.)
2 Engineering Technology Research Center for Intelligent & Low-Carbon Assembled Building, Shijiazhuang 050018, China
3 State Key Laboratory of Building Safety and Built Environment, Beijing 100013, China; lihao@emcso.com
4 China Academy of Building Research, Beijing 100013, China
* Correspondence: wangzc@emcso.com

Abstract: To achieve the goal of carbon peaking, it is crucial to reduce both carbon emissions and energy consumption during the operational stage of residential buildings. This paper proposed a method for assessing carbon emissions and energy consumption for an energy system utilized in a rural residence. First, an equivalent thermal resistance-capacitance model for a rural residence was established. The parameters of thermal resistance and capacitance were optimized based on the data collected from an operating air source heat pump heating system. On this basis, the energy consumption was derived, and it was compared with real consumption. Then, a method of estimating house energy consumption index per unit area under specified weather conditions was proposed. Finally, the carbon emissions of three heating types—heating driven by air source heat pump, gas boiler, and coal boiler—were compared. Results showed that the derived energy consumption index per unit area was 46.77 W/m^2. The carbon emissions of the air source heat pump were 1406.1 kgCO_2.

Keywords: carbon emissions; energy consumption index; equivalent thermal resistance-capacitance model; air source heat pump; parameter estimation

Citation: Kang, L.; Li, H.; Wang, Z.; Wang, J.; Sun, D.; Yang, Y. Investigation of Energy Consumption via an Equivalent Thermal Resistance-Capacitance Model for a Northern Rural Residence. *Energies* **2023**, *16*, 7835. https://doi.org/10.3390/en16237835

Academic Editors: Vincenzo Costanzo and Francesco Minichiello

Received: 24 September 2023
Revised: 28 October 2023
Accepted: 20 November 2023
Published: 29 November 2023

1. Introduction

In recent years, the intensification of the greenhouse effect resulting from massive CO_2 emissions has been identified as a fundamental cause of global warming [1]. China has announced the implementation of more effective policies and measures, with the aim of achieving a carbon emissions peak before 2030 [2]. Building energy consumption, as one of three major energy consumers, plays an important role in energy saving and emissions reduction [3].

Building full life cycle decarbonization was a comprehensive approach that involved optimizing an entire building's life cycle to minimize carbon emissions [4]. By evaluating the entire life cycle of buildings, policies for energy conservation and carbon emissions reduction were developed to achieve the goal of reaching peak carbon as soon as possible. Luo et al. [5] analyzed three public buildings—office, hospital, and school—g to quantitatively study the impact of factors such as structure, materials, architectural life, and other factors on carbon emissions. Xu et al. [6] proposed a complete optimization method for achieving energy-efficient and low-carbon schools throughout their entire life cycle based on evaluation indexes of energy saving and life cycle decarbonization. Oscar et al. [7] made a comparative analysis of the energy consumption and environmental impact of residential buildings in Spain and Colombia through life-cycle evaluation, revealing that the building envelope was a key factor affecting energy consumption and carbon emissions.

Biswas et al. [8] analyzed the life-cycle carbon emissions of an engineering museum and discovered that the use of a sophisticated building management system could achieve nearly 63% emissions reduction during operation. Luo et al. [9] established a life-cycle optimization approach that considers the increase in embodied energy and carbon for a comprehensive assessment of economic, energy, and environmental performance. In a comparative analysis of the life-cycle cost and carbon emissions of typical commercial buildings, Kneifel et al. [10] found that the selection of building materials and technologies had a significant impact on carbon emissions. In a life-cycle assessment of a typical office building in Norway, Rabani et al. [11] discovered that retrofitting measures resulted in a reduction of total net emissions by up to 52%.

Moreover, carbon and energy software as well as building information modeling (BIM) were also utilized to calculate and analyze life-cycle carbon emissions. Zhang et al. [12] proposed a BIM-based approach for integrating life cycle carbon emissions and costs of public buildings, while Peng et al. [13] estimated life cycle carbon emissions of an office building using Ecotect and BIM.

For predicting and modeling building carbon emissions, Liang et al. [14] proposed a rapid assessment model to reduce operational carbon emissions for commercial buildings. Zhang et al. [15] used scenario analysis based on the long-range energy alternatives planning system model to predict carbon emissions in public buildings in China. Verbeeck et al. [16] proposed a life-cycle inventory model and analyzed energy consumption and carbon emissions of five different forms of residential buildings. Shao et al. [17] conducted systematic carbon accounting to estimate carbon emissions of a specific building in Beijing economic-technological development area. Iddon et al. [18] utilized BIM to estimate carbon emissions during the operational phase of a typical four-bedroom detached house. Zhang et al. [19] and Zhu et al. [20] employed a process-based approach to estimate carbon emissions from the construction sector in China. Gan et al. [21] and Mao et al. [22] used a process analysis method and determined carbon emissions per unit area of the building. Zhang et al. [23] proposed an input-output method to calculate carbon emissions of urban building stock. Employing Monte Carlo simulation based on input-output analysis, Acquaye et al. [24] analyzed solidified carbon emissions from apartment buildings.

Literature reviews showed that the study of carbon emissions mainly concentrated on life cycle evaluation, and its modeling usually relied on the entire building, while carbon emissions during the operational stage accounted for 70–82% of overall life-cycle emissions in the building industry [25]. Therefore, investigating and reducing these carbon emissions is crucial to achieving the carbon peak goal. Lomas et al. [26] and Rogers et al. [27] studied the emissions reduction of existing buildings and gave corresponding carbon emissions reduction suggestions. Airaksinen et al. [28] studied a new office building through the design schemes and provided different alternatives to influence building energy consumption and CO_2-equivalent emissions of energy implied by building materials. Ye et al. [29] conducted a detailed analysis of carbon emissions resulting from heating and cooling systems in urban residential buildings.

In this paper, a data-driven method to estimate energy consumption and carbon emissions of a building's energy system is proposed through the gray box thermal model. To predict energy consumption of a rural residence, an equivalent thermal resistance-capacitance model was established, and parameters of thermal resistance and capacitance were optimized based on data collected from employed air source heat pump heating system. On this basis, energy consumption is predicted, and energy consumption index per unit area under specified weather is derived. Moreover, according to carbon emissions factors of different energy, carbon emissions of different heating types are deduced.

2. Experimental Methodologies

The experiments are carried out in a rural residence in Beijing. Figure 1 shows the view of the experimental residence, which is a one-story house with a total covered area of about 120 m^2. It faces south and was built in 2005, and the envelope structure is comprised

of traditional concrete wall structures. The heat absorption and emissions of items such as furniture are not considered. Between 10 p.m. and 6 a.m., no equipment or facilities are operated. In winter, the heating load is satisfied by an ASHP with fixed speed produced by OUTES in 2018. Table 1 lists the nameplate parameters of the selected ASHP.

Figure 1. View of experimental residence in rural Beijing.

Table 1. Nameplate parameters of the fixed speed ASHP used in residence.

Parameter	Symbol	Unit	Value
Nominal cooling capacity	Q_c	kW	10.0
Nominal coefficient of performance (cooling mode)	COP_c	—	2.44
Nominal heating capacity	Q_h	kW	14.5 [1]/9.1 [2]
Nominal coefficient of performance (heating mode) [1]	COP_h	—	3.22 [1]/2.32 [2]
Rated flow rate of water	m	m^3/h	1.56

Note: [1] represents the following test conditions: outdoor dry bulb temperature, outdoor wet bulb temperature, and supplied water temperature are 7 °C, 6 °C, and 45 °C, respectively. [2] represents the following test conditions: outdoor dry bulb temperature, outdoor wet bulb temperature, and supplied water temperature are −12 °C, −14 °C, and 41 °C, respectively.

Figure 2 shows the schematic diagram of a heating system driven by ASHP and its data acquisition system. The monitoring data for training and validation include outdoor temperature (T_{out}) and indoor temperature (T_{in}), supplied water temperature (T_s) and returned water temperature (T_r), water flow rate (m), and system power consumption (P). Heating load provided by ASHP will be calculated based on the measured water flow rate and temperature difference between supplied water and returned water.

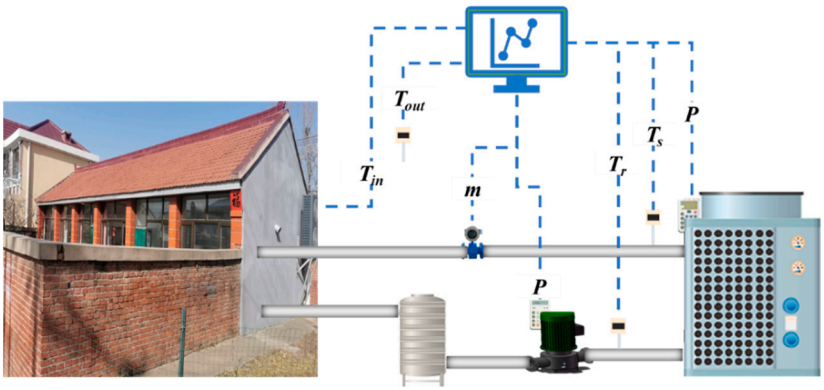

Figure 2. Schematic diagram of ASHP heating system and its data acquisition system.

To measure outdoor temperature, the thermocouple is located at 1.5 m above ground and 20 cm from the external surface of wall. When measuring indoor air temperature, the thermocouple point is placed at the lower surface of the desk. These positions are protected from interference caused by the inlet and outlet flow of the air source heat pump unit, as well as from direct sunlight irradiation [30]. It is also arranged at the inlet and outlet of the ASHP water system to measure the temperature of supplied and returned water. An electromagnetic flow meter is employed, and it is located at the pipe of the supplied water to obtain the water flow rate. The measurement instruments and corresponding

accuracy are listed in Table 2. Before testing, all instruments and equipment used during the experiment are calibrated. The measured data are sampled every 1 min from 22:00 of the previous day to 6:00 of the next day. This sampling interval is sufficiently small, which can prevent thermal dynamics overlooking.

Table 2. Measurement instruments and corresponding accuracy.

Sensor		Measurement	Accuracy
Thermometer	*RTD*	T_{out}	±0.5 °C
	NTC	T_{in}	±0.5 °C
	RTD	T_s, T_r	±0.2 °C
Electromagnetic flow meter		m	2%
Electronic watt-hour meter		W	±1%

3. Modeling and Methodology

Figure 3 shows the prediction process of energy consumption and carbon emissions. It mainly includes data collection, data pre-processing, resistance-capacitance model (RC model) establishment, and corresponding energy consumption and carbon emissions prediction.

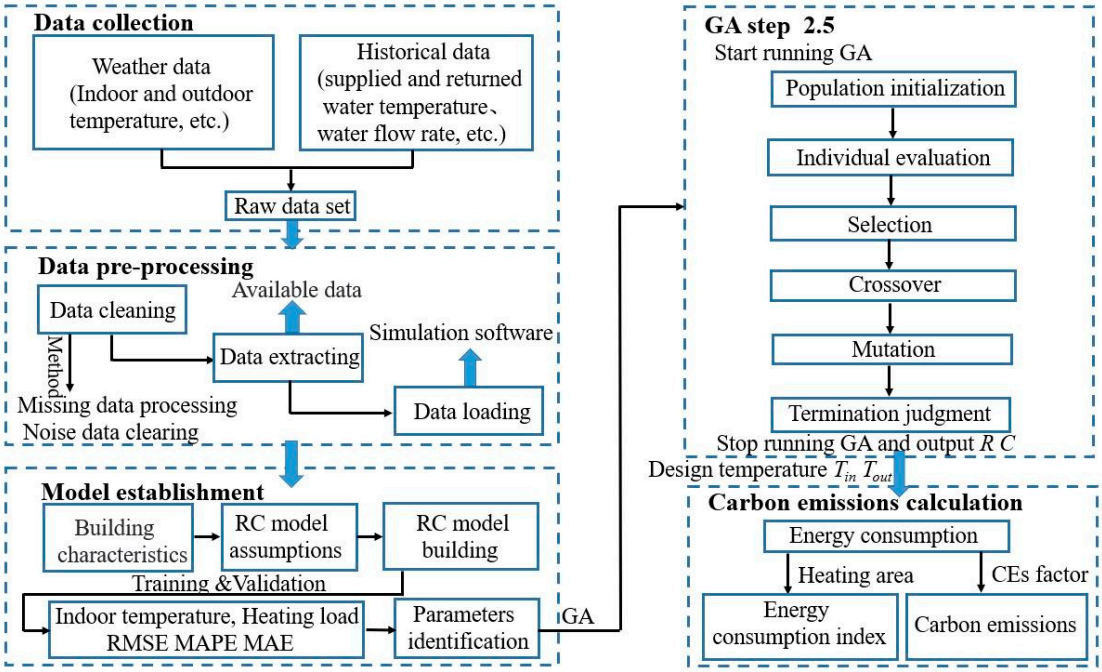

Figure 3. Prediction process of energy consumption and carbon emissions based on RC model.

3.1. RC Structure (Assumptions and RC Model)

The RC model is a lumped parameter model, in which the house is regarded as a whole. While the thermal process in a house is complex, particularly with regard to radiation between surfaces at different temperatures, the equivalent RC model provides a simplified representation.

The development of an equivalent RC model for a house entails the consideration of heat transfer, including the following:

(1) Heat transfer between indoor and outdoor air through an opaque envelope

The opaque envelope includes the exterior walls and roof. It has the effects of heat preservation and heat insulation, especially in the wall with an insulated material layer. Thus, the state of the indoor air dry-bulb temperature has a certain attenuation and delay

relative to the outdoor air dry-bulb temperature. The exterior walls and roof are considered as a whole, and it is divided into several layers on a one-dimensional space from outdoor to indoor as needed. The number of layers is the amount of thermal resistance R in the equivalent RC model.

When constructing the equivalent "xRyC" model, the model complexity should be considered. If it is detailed with a finite difference model, it will be more difficult to calculate. If the simplest 1R1C is considered, it will be difficult to distinguish the heat storage effect on the opaque envelope and indoor air. The 2R1C model is widely employed in building opaque envelopes to achieve effective control over heat, humidity, and energy within structures. In references [31–33], the 2R1C model was used to simplify the opaque envelope, and satisfactory results were obtained. Thus, in this paper, the equivalent RC model of the opaque envelope is simplified into a 2R1C structure as shown in Figure 4. In Figure 4, T_{oe} is the temperature of the opaque envelope. R_{out} and R_{in} are the thermal resistance between the indoor air and interior surface and the resistance between the exterior surface and outdoor air, respectively. C_{oe} is the thermal capacitance of the opaque envelope.

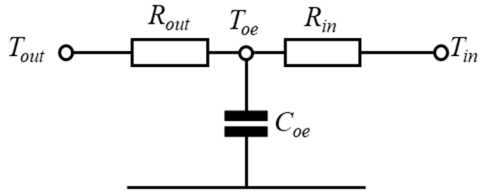

Figure 4. Equivalent RC model of opaque envelope.

(2) Heat transfer through the transparent envelope

The transparent envelope consists of external windows and glass curtain walls. The heat transfer through the transparent envelope mainly includes two parts, heat transfer driven by the temperature difference between indoor and outdoor air and heat gains from solar radiation. Due to little thermal capacity, the transparent envelope acts as thermal resistance. For heat transfer driven by the temperature difference between indoor and outdoor air, the transparent envelope is considered as a whole and is seen as one thermal resistance. The simplified equivalent RC model of the transparent envelope is shown in Figure 5, where, R_{inf} is the thermal resistance between indoor and outdoor air through the transparent envelope.

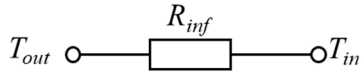

Figure 5. Equivalent RC model of transparent envelope.

Moreover, there may be some gaps between the transparent envelope and the opaque envelope; infiltrated air has to be heated or cooled to make indoor air temperature constant. Thus, in this paper, the influence of heat transfer attributed by infiltrated air is put into the parameter of thermal resistance R_{inf}.

The solar radiation through the transparent envelope is a part of the solar radiation on the house, and there is a proportional relationship with the solar radiation illuminance on a horizontal direction. Considering the indefinite rate of solar radiation for each indoor area, only the data obtained at night are employed to train and test, so the factor of solar radiation is excluded in the model.

(3) Heat transfer from internal heat source and energy supply system

Internal heat sources include the human body, lights, equipment, etc. Considering that lights and equipment are mostly off, and people fall asleep during the night, the heat gains from these internal heat sources are not embodied in the equivalent RC model.

Moreover, in order to maintain a comfortable heat and humidity environment, energy must be supplied. The indoor air temperature will be regulated through an energy supply system. Thus, the supplied energy is settled as a boundary condition of the equivalent RC model. Taking the ASHP heating system as an example, the supplied heat is as follows:

$$Q_{ASHP} = \rho m c_p (T_s - T_r) \quad (1)$$

where ρ and c_p are the density and specific heat of water, respectively.

(4) Indoor air and internal thermal mass

Compared with the wall and other building structures, the thermal capacity of indoor air is small. However, it is the most direct material carrier of indoor temperature. Indoor space composed of indoor air is a key part of the human body perceiving temperature changes, and the heat capacity of indoor air should be reflected in the RC model.

Internal thermal mass includes the floor, ceiling, internal partition wall, furniture, etc. It can receive radiation heat from solar radiation, internal heat sources, and the energy supply system. Logically, heat can be stored in internal thermal mass, and when its temperature is higher than indoor air temperature, the stored heat will be released to regulate indoor air temperature. Thus, one equivalent thermal capacity is employed to represent internal thermal mass, and one thermal resistance is put forward to distinguish the different temperature between indoor air and internal thermal mass.

The equivalent RC model between internal thermal mass and indoor air is shown in Figure 6, where T_m is the temperature of internal thermal mass, R_m is the thermal resistance between internal thermal mass and indoor air, And C_{in} and C_m are the thermal capacitance of indoor air and internal thermal mass, respectively.

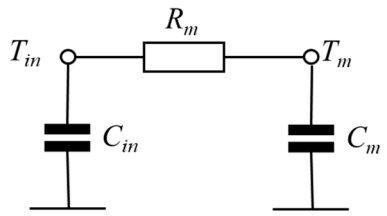

Figure 6. Equivalent RC model of internal thermal mass and indoor air.

3.2. Equivalent RC Model for Rural Residence

To build a thermal balance equation of the equivalent RC model and the simple equivalent RC model for calculations, the following simplified assumptions are made:

(1) Heat generation or accumulation within the house construction elements does not exist. The temperature of surface segment or whole surface is uniform within its cross section. Thus, the heat transfer can be regarded as a one-dimensional process.
(2) The effect of meteorological parameters, including wind velocity, on heat transfer is negligible. Hence, the thermal resistance or heat transfer coefficient is assumed to be constant. On the side, the effect of temperature and humidity on thermal capacity is not considered; the related thermal capacitance is assumed to be constant.
(3) The experiment is carried out during the night, so the heat from solar radiation or internal heat source is negligible. Hence, the surface temperature of internal thermal mass is assumed to be equal to the indoor air temperature. Correspondingly, the thermal capacitance of the internal thermal mass is summarized to indoor air capacity.
(4) Indoor air is well mixed and homogeneous, so it is assumed to be at a uniform temperature.

Combined with the RC model formulation in Section 3.1, an equivalent 3R2C model for the rural residence is presented, which is shown in Figure 7.

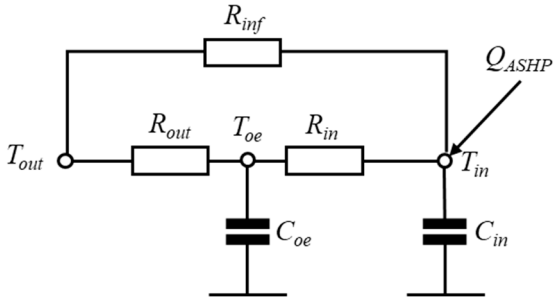

Figure 7. Equivalent 3R2C model of the rural residence.

The governing equations at each node obtained by heat balance in Figure 7 are as follows:

$$C_{oe}\frac{dT_{oe}}{dt} = \frac{T_{out} - T_{oe}}{R_{out}} + \frac{T_{in} - T_{oe}}{R_{in}} \tag{2}$$

$$C_{in}\frac{dT_{in}}{dt} = \frac{T_{out} - T_{in}}{R_{\text{inf}}} + \frac{T_w - T_{in}}{R_{in}} + Q_{ASHP} \tag{3}$$

3.3. Evaluation Indexes

Evaluation indexes are essential to estimate the results of parameter prediction. In this paper, mean absolute error (*MAE*), mean absolute percentage error (*MAPE*), and root-mean square error (*RMSE*) are employed to evaluate the accuracy of parameter prediction. The difference between predicted results and the real test value can be reflected from different aspects. They are defined as follows:

$$MAE = \frac{1}{N}\sum_{i=1}^{N}\left|x_{act} - x_{pre}\right| \tag{4}$$

$$MAPE = \frac{1}{N}\sum_{i=1}^{N}\left|\frac{x_{act} - x_{pre}}{x_{act}}\right| \tag{5}$$

$$RMSE = \sqrt{\frac{1}{N}\sum_{i=1}^{N}\left(x_{act} - x_{pre}\right)^2} \tag{6}$$

3.4. Optimization Method

From the constructed equivalent 3R2C model, there is a nonlinear optimization process to acquire the optimal values of *R* and *C*. The optimization problem can be solved through many methods, such as the direct exhaustive search method, sequential quadratic programming, and genetic algorithm (GA). For global optimal problems, GA presents good robustness, especially in solving multi-objective and multi-modal optimization problems [34]. It has been widely used in heating, ventilation, and air conditioning systems to obtain global optimal solutions [35]. Therefore, it is also employed to search for the optimal values of *R* and *C* based on the equivalent 3R2C model built for the rural residence.

Figure 8 shows the flowchart of the GA optimization method. In GA, the chromosome of an individual includes five parameters (R_{out}, R_{in}, R_{inf}, C_{oe}, C_{in}). The search space of these parameters is their own respective setting ranges. Table 3 shows some of GA optimization settings, and the fitness function of GA optimization is as follows:

$$f(R_{out}, C_{oe}, R_{in}, R_{inf}, C_{in}) = \frac{1}{\sqrt{\frac{1}{N}\sum_{i=1}^{N}\left(x_{act} - x_{pre}\right)^2}} \tag{7}$$

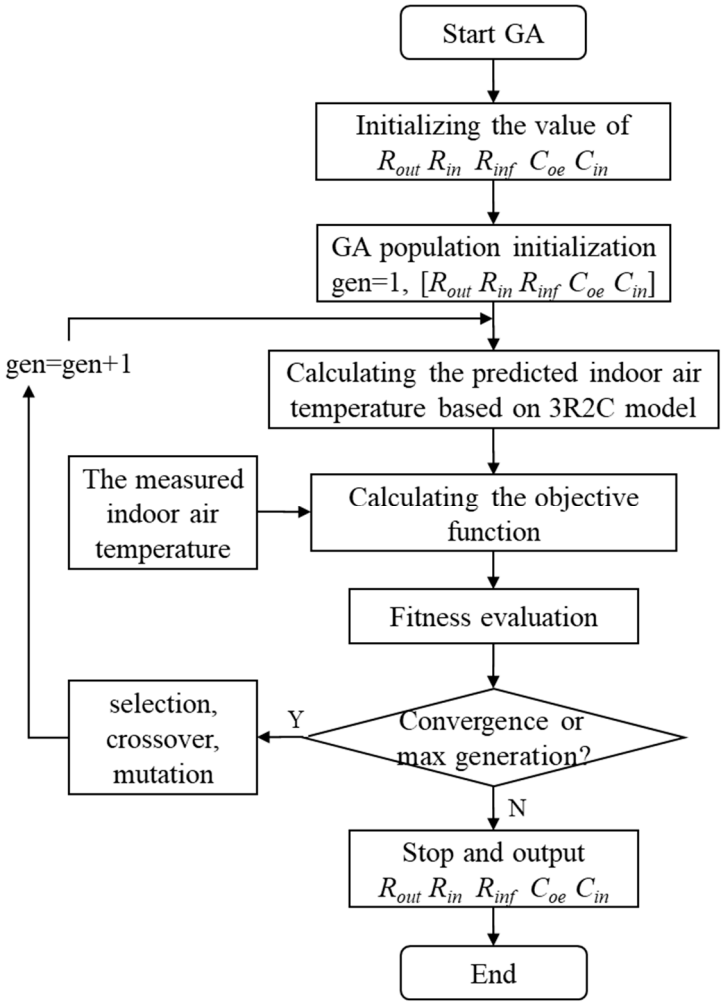

Figure 8. Flowchart of GA optimization method.

First, before the optimization process of GA is carried out, the specific parameters *R* and *C* of the problem need to be estimated. Specific constraints and objectives of the problem, such as constraints and objective functions in optimization problems, are often represented by *R* and *C*. The initial population is produced by initializing the five parameters to start GA optimization. Then, the indoor air temperature is predicted by the 3R2C model of the rural residence, and fitness function is calculated. The fitness function will serve as the criterion for determining the survival of individuals with superior traits. Following that, the next generation population is produced through a crossover and mutation process, and the fitness is evaluated too. After the selection, crossover, and mutation of the population, a new generation is formed through reconstitution, resulting in acquisition of the next generation population. Additionally, gen = gen + 1. At this step, the elitist and best fitness will be recorded. The criterion to terminate GA optimization is whether the number of current generations is larger than the pre-set maximum number or the difference of the best fitness values between two consecutive runs is less than the sett threshold value.

Table 3. GA optimization settings.

Sensor	Value
Population Size	400
Generations	800
Crossover Fraction	0.8
Mutation Fraction	0.2

3.5. Model of Carbon Emissions

The energy consumption can be obtained by Equation (1), while carbon emissions can be calculated as follows:

$$CE = Q \times CEF \tag{8}$$

$$CE_0 = \frac{CE}{A} \tag{9}$$

where CE and CE_0 are total carbon emissions and carbon emissions per unit area, respectively. Q is the energy consumption and CEF is the carbon emissions factor of the corresponding energy. A is the serviced area.

4. Results and Discussion

In this section, the experimental data are utilized for training and validation to derive R and C in the 3R2C model. On this basis, energy consumption is also predicted, and then a method for calculating the energy consumption index under standard meteorological conditions as well as carbon emissions is proposed. Limitations and future research of this study are also presented in this section.

4.1. Training Results

As Section 3.2 showed, the heat from solar radiation and internal heat sources is not included in the model, as data during 22:00 and 6:00 are selected as the driven data to train R and C. To predict indoor air temperature using the equivalent 3R2C model, the data including outdoor and indoor air temperature, supply and return water temperature, and water flow rate need to be tested first. Generally, more training data will provide more robust results, although testing more data requires more waiting time for the model to function properly. Therefore, the amount of data collection time required is firstly examined to obtain sufficiently reliable results for parameter estimation (R and C optimization). Figure 9 shows testing data from a fixed speed ASHP system in a rural residence in Beijing.

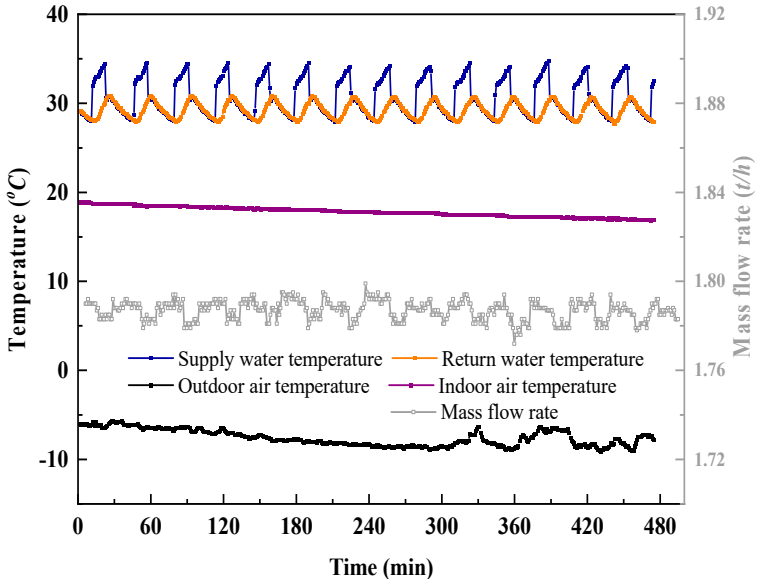

Figure 9. Actual measured data used for training.

Because fixed speed ASHP is employed, it can be seen that water flow rate is almost constant; the supplied heat is controlled through the on-off state of the compressor. During the ON period, the supplied heat of the ASHP is higher than the heat diffusion of the terminal, and the supply and return water temperatures increase until the controller detects the return water temperature reaching the upper limit and switches off the compressor.

During the OFF period, the supply and return water temperatures decrease until the controller switches on the compressor when it detects that the return water temperature drops beyond the lower limit. On account of the constant water flow rate as well as the heating load, the change trend of the indoor air temperature is similar to that of the outdoor temperature. The outdoor temperature ranges between −9.1 °C and −5.7 °C, and the indoor air temperature ranges between 17 °C and 19 °C.

The training was initiated by using one hour's testing data to estimate *R* and *C*. Then, estimation of the parameters is repeated incrementally by adding one hour's training data sets per trial, i.e., the first trial employs training data of the first hour, the second trial employs training data of the first two hours, and the eighth trial uses training data of whole night. Figure 10 shows the predicted and actual measured indoor air temperature based on different training times. Table 4 shows the correlation coefficient and error results of different training times.

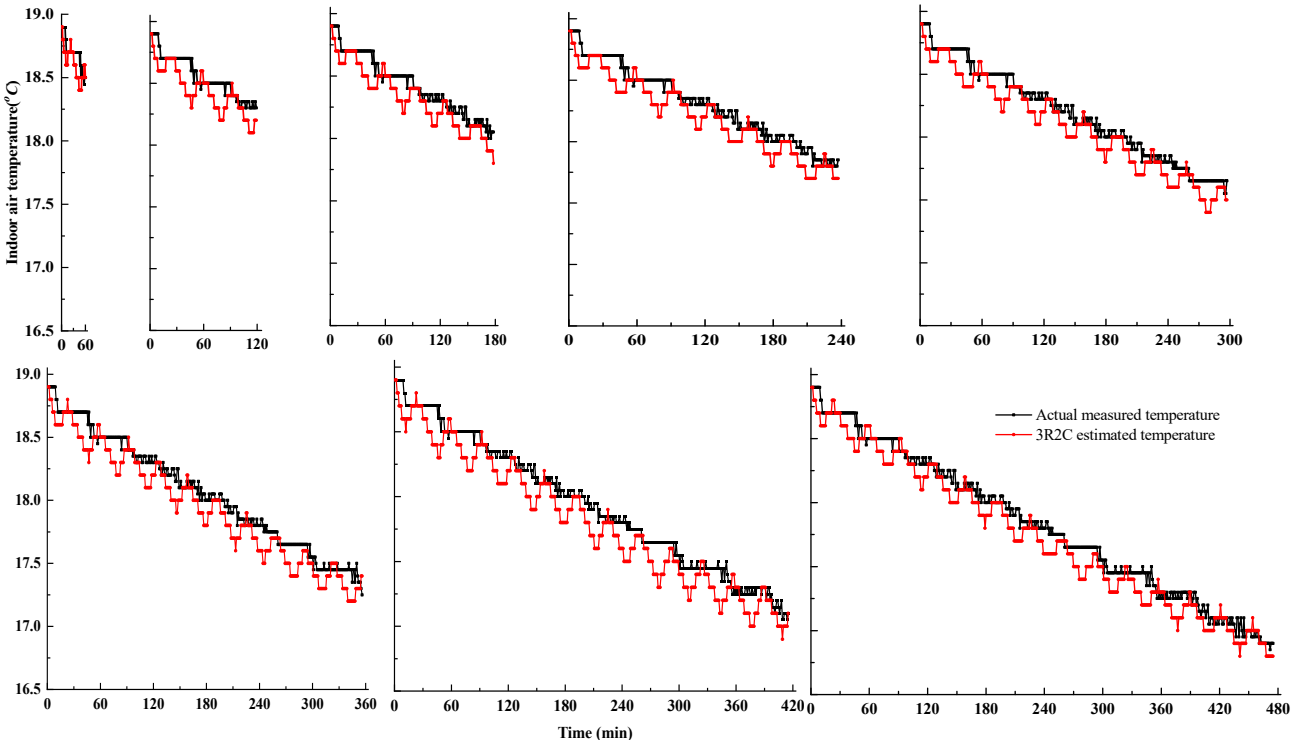

Figure 10. Predicted vs. actual indoor air temperature based on different training times.

Table 4. Correlation performances and error results of different training times.

Training Time (min)	*R* (%)	*Cov* (%)	*MAE* (%)	*MAPE* (%)	*RMSE* (%)
60	63.15	0.92	10.08	0.55	12.98
120	81.12	2.54	12.48	0.67	16.02
180	92.38	5.28	11.01	0.60	14.08
240	95.45	8.74	10.55	0.58	13.48
300	96.99	13.05	10.59	0.58	13.32
360	97.44	18.43	11.99	0.66	14.81
420	97.71	24.22	13.29	0.74	16.44
480	98.75	30.99	9.79	0.55	12.26

It can be seen that the predicted indoor air temperatures match the actual measured indoor air temperatures well. With the increasing of training time, better following quality is presented, and correlation performance is better. When the training data increases to

four hours, the correlation coefficient is 95.45%, and covariance increases to 8.74%. When the sampling data increase to the whole night, the correlation coefficient and covariance reach 98.75% and 30.99%, respectively. In addition, as shown in Table 4, *MAE*, *MAPE*, and *RMSE* first increases and then decreases with the increase of training data. The reason may be that there is a little fluctuation in the outdoor temperature between the sixth and seventh hours. The minimum *MAE*, *MAPE*, and *RMSE* are obtained by the training using eight-hour training data, which are 9.79%, 0.55%, and 12.26%, respectively. Table 5 shows the estimation results of the parameters for different training times. As shown in Table 5, the five parameters exhibit fluctuations within a certain range as the training time increases. Among them, R_{out} and C_{in} demonstrate the most significant fluctuation range, ranging from 7.93 K/W to 17.34 K/W and from 221.48 J/K to 299.71 J/K, respectively. The remaining three parameters undergo minimal changes.

Table 5. Estimation results of the parameters for training optimization.

Training Time (min)	R_{out} (K/W)	C_{oe} (J/K)	R_{in} (K/W)	R_{inf} (K/W)	C_{in} (J/K)
60	11.86	3.25	3.37	8.54	299.71
120	10.73	3.96	3.21	10.92	243.18
180	9.79	4.05	3.09	10.50	278.82
240	17.34	3.17	3.25	8.15	272.57
300	11.97	3.88	3.17	9.52	277.42
360	12.81	3.37	3.35	9.51	246.08
400	7.93	3.80	3.26	13.39	221.48
480	18.18	2.72	3.43	7.73	288.41

4.2. Validation Results in the Same Operation Period

Figure 11 shows indoor air temperature validation results conducted in the same period with those of training data. It can be seen that in the same operation period, the predicted indoor air temperature can follow the trends of actual measured indoor air temperature well. Except for the estimation results of the one-hour training time, the errors including *MAE*, *MAPE*, and *RMSE* are comparatively small. The minimum *MAE*, *MAPE*, and *RMSE* are obtained by the estimation of the parameters of the two-hour training time, which are 13.98%, 0.78%, and 16.99%, respectively. With the increase of training time, the error results change little and fluctuate at a certain level. When the parameter estimation results of the eight-hour training time are used, the *MAE*, *MAPE*, and *RMSE* are 16.96%, 0.95%, and 19.71%, respectively, while the correlation coefficient and covariance increase to 98.13% and 29.19% from 97.32% and 25.61%, respectively.

4.3. Validated Results in Other Operation Periods

For the combined results of Sections 3.1 and 3.2, considering the lower error of the eight-hours training time and estimation results for the parameters under different training times, validation in the other four different operation periods are conducted based on estimation results for the parameters of the eight-hour training time.

Figure 12 shows the actual measured profiles of the other four different operation periods. The weather of these four operation periods is defined as severe cold, cold, cool, and mild weather. It can be seen that in severe cold weather, outdoor air temperature changes between −14.5 °C and −8.4 °C, while in cold, cool, and mild weather, it changes between −9.7 °C and −3.6 °C, −4.9 °C and −0.5 °C, and 0.1 °C and 5.2 °C, respectively. However, on account of the same ASHP system and the same heating load, indoor air temperature is different. For example, it changes between 14.3 °C and 16.1 °C under severe cold weather and 21 °C and 23 °C under mild weather.

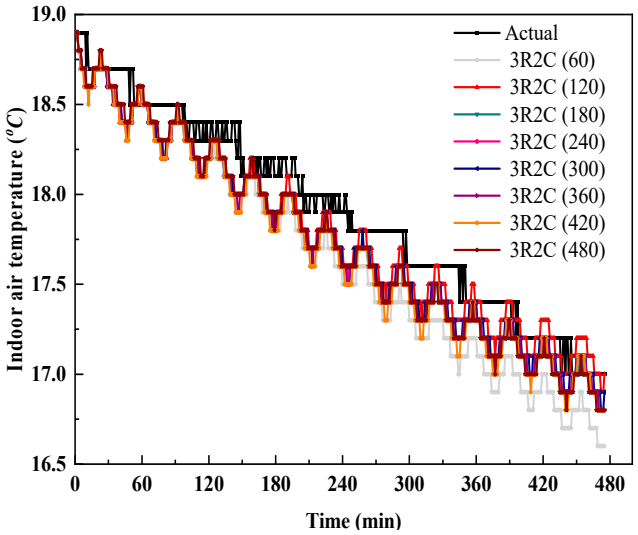

Figure 11. Predicted vs. actual measured indoor air temperature (validation in the same operation period).

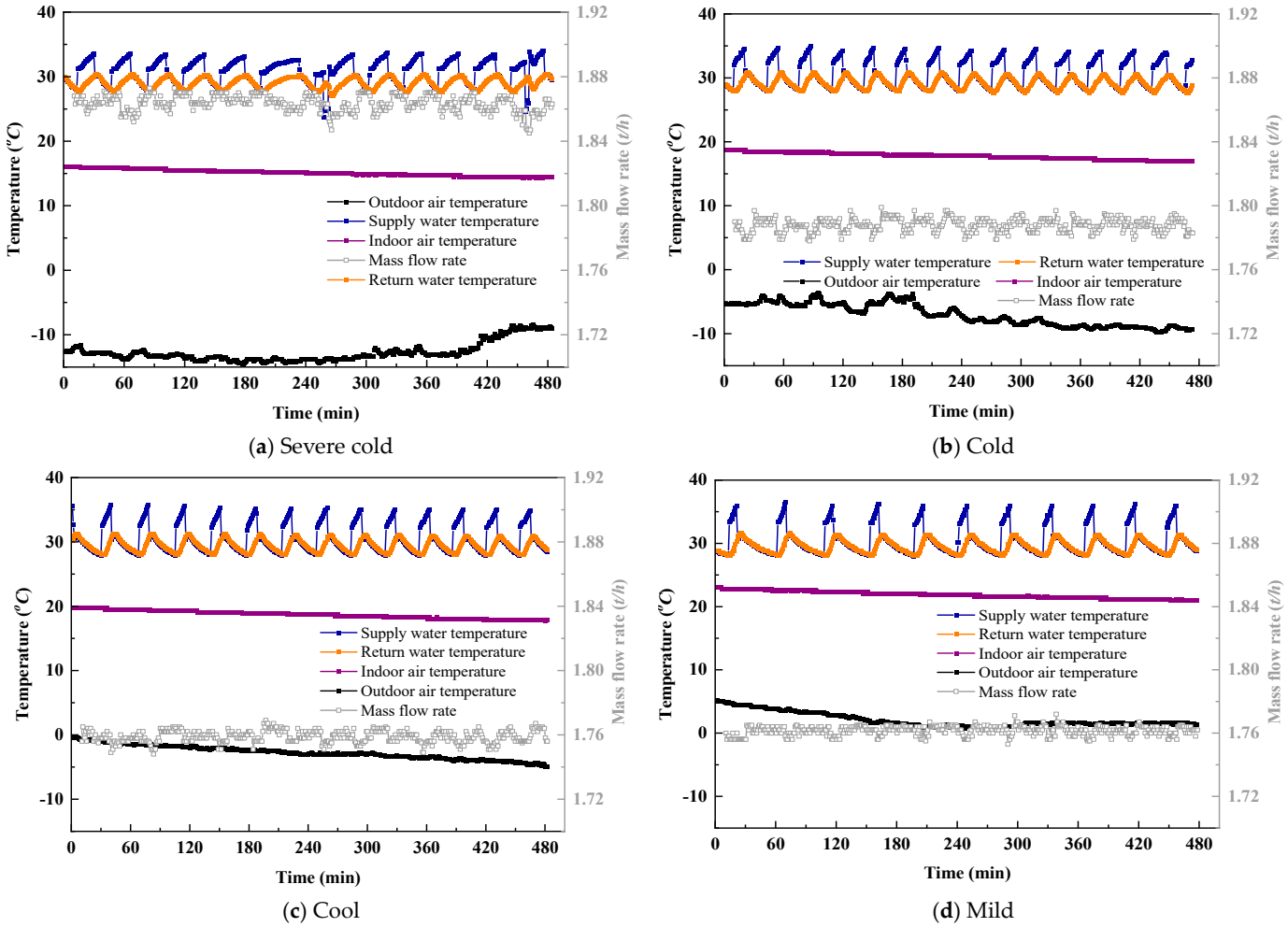

(**a**) Severe cold (**b**) Cold

(**c**) Cool (**d**) Mild

Figure 12. Actual measured data used for validation.

Figure 13 shows the predicted and actual measured indoor air temperature under the other four operation periods. Table 6 presents the error results of validation. It can be seen that the predicted indoor air temperature matches the actual indoor air temperature and its dynamic trend well. Combined with Table 6, under all weather conditions, the

correlation coefficient is beyond 96% and the covariance is more than 20%. The minimum value of *MAE* is obtained under cold weather, which is 8.25%. Under severe cold, cool, and mild weather, the *MAE* values are 15.05%, 19.07%, and 9.75%, respectively. For *MAPE* and *RMSE*, the minimum values are obtained under mild weather. Under severe cold, cold, cool, and mild weather, the *MAPE* values are 0.99%, 0.95%, 1.03%, and 0.45%, respectively, and the *RMSE* values are 17.91%, 19.71%, 23.32%, and 12.53%, respectively.

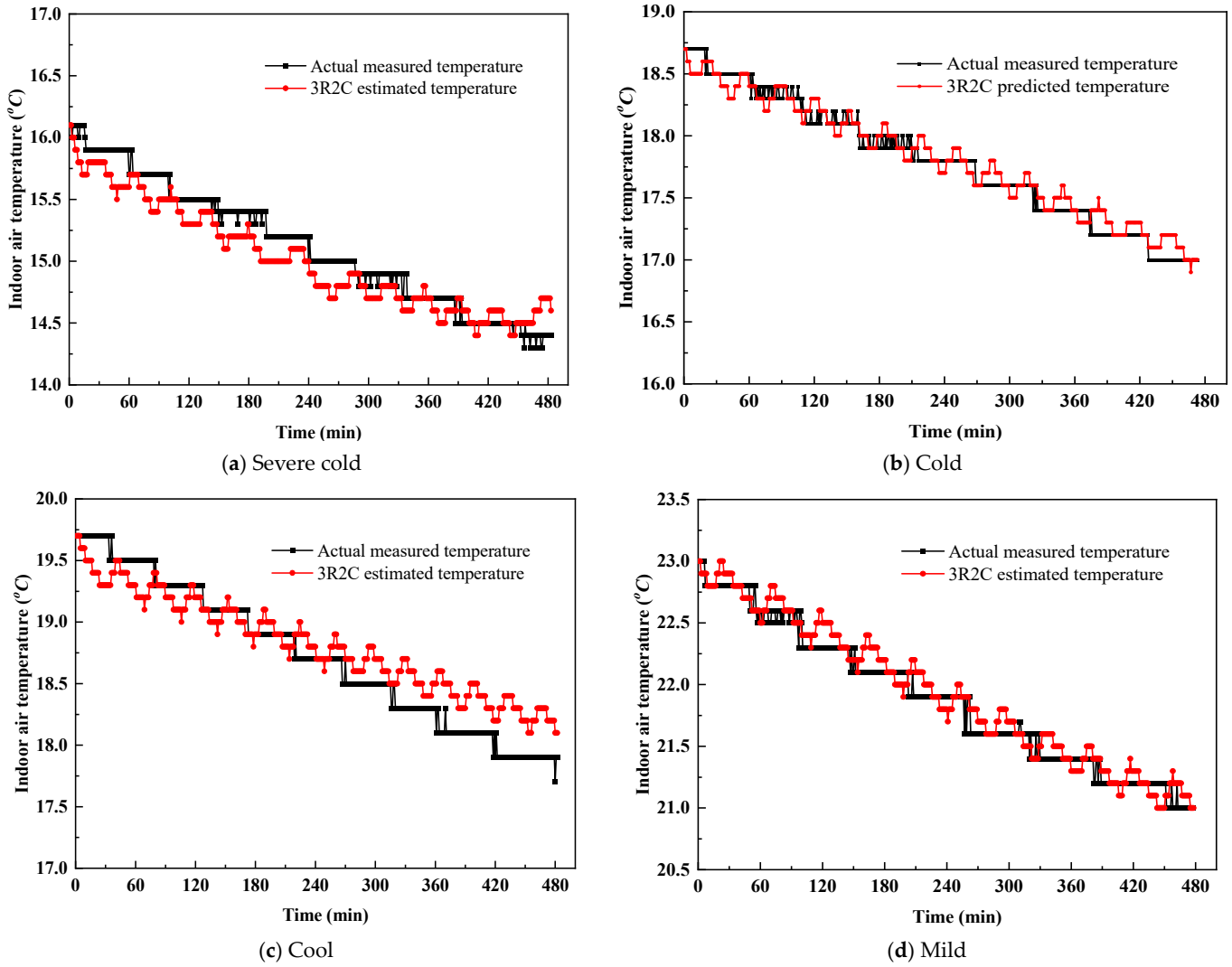

Figure 13. Predicted vs. actual measured indoor air temperature (validation in the other four operation periods).

Table 6. Validation results in the other four operation periods.

Weather Type	Outdoor Temperature Range	*R*	*Cov* (%)	*MAE* (%)	*MAPE* (%)	*RMSE* (%)
Severe cold	−14.5~−8.4	0.9663	20.38	15.05	0.99	17.91
Cold	−9.7~−3.6	0.9800	22.20	8.25	0.95	19.71
Cool	−4.9~−0.5	0.9701	21.74	19.07	1.03	23.32
Mild	0.1~5.2	0.9800	31.38	9.75	0.45	12.53

4.4. Estimation of Energy Consumption

Using the estimation results of the parameters of *R* and *C*, the energy consumption of the rural residence can be predicted. Figure 14 shows the predicted and actual energy

consumption of the same period with the training case and the other four different operation periods. It can be seen that regardless of the meteorological condition, the obtained energy consumption deduced by optimized 3R2C results follows the actual energy consumption well. Statistical results show that the *MAPE* of the same period a the training case is 7.09%. Under the meteorological conditions of severe cold, cold, cool, and mild, the *MAPE* values are 8.74%, 4.28%, 12.56%, and 9.88%, respectively. Under the meteorological condition of cold, the error is minimal because the meteorological condition is similar to the condition of the training case. The error under the meteorological condition of cool is higher because in its first validation hour, the ASHP is not operated most of the time, and the accumulated actual energy consumption is less, while the predicted energy consumption exists continuously when the temperatures of the indoor air, outdoor air, and envelope are different. Thus, in the first hour, the deviation between accumulated actual energy consumption and predicted energy consumption is larger. With the accumulated time increasing, the deviation becomes small.

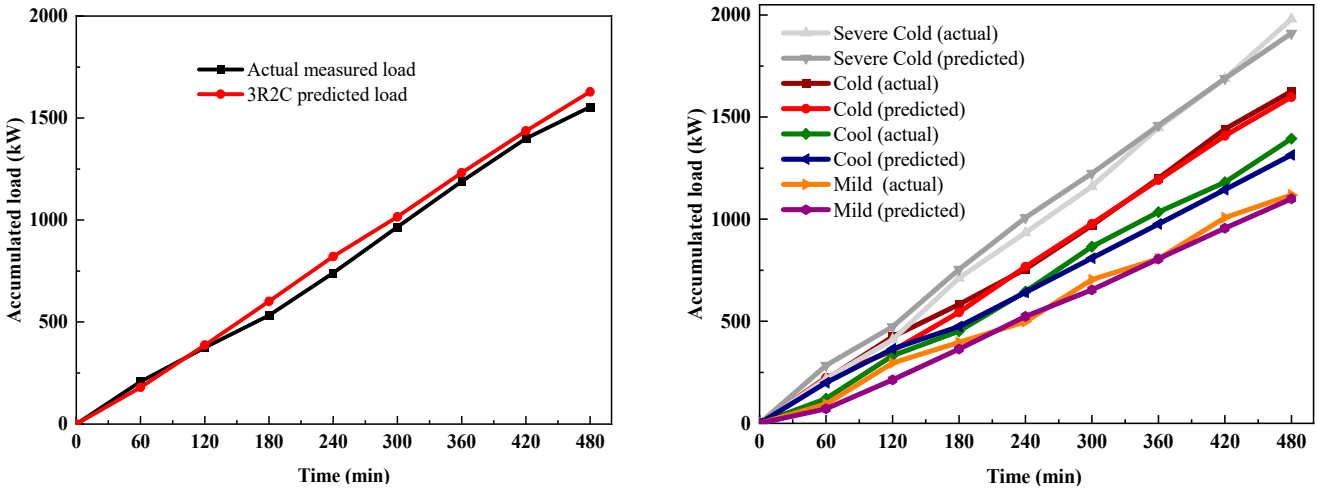

(**a**) Training case (**b**) Validation case

Figure 14. Predicted and actual energy consumption.

Moreover, this method can be employed to estimate whether the energy consumption conforms to the energy saving standard. In Beijing, the outdoor design temperature for heating is −7.6 °C. If the indoor air temperature is set at 18 °C, the energy consumption can be deduced, and it is 4.49 kW. If the heating area is assumed as 80% of the house area, the energy consumption index is 46.77 W/m^2, correspondingly.

In the literature [36], field monitoring was carried out on 103 household ASHP systems in rural residences around Beijing in the 2018–2019 heating season. Analysis of the statistical data and selected typical cases showed that the average values of heating load per unit area on the coldest day and over the entire heating season were 54.7 W/m^2 and 44.3 W/m^2, respectively. The obtained result in this paper is consistent with that of [36], which, in another point of view, expresses that the proposed method to estimate energy consumption is effective. Thus, the obtained energy consumption can be utilized to calculate carbon emissions.

4.5. Estimation of Carbon Emissions

Table 7 presents the carbon emissions factors of three heating types: heating driven by ASHP, gas boiler, and coal boiler, respectively. It can be seen that the carbon emissions factors of electricity, gas, and coal are 0.604 tCO_2/MWh, 0.0555 tCO_2/GJ, and 0.089 tCO_2/GJ, respectively.

Table 7. Carbon emission factors of various heating types—[37].

Heating Type	Carbon Emission Factor	Unit
ASHP	0.604	tCO_2/MWh
Gas boiler	0.0555	tCO_2/GJ
Coal boiler	0.089	tCO_2/GJ

To calculate carbon emissions of each heating type, it is assumed that the COP of ASHP and the efficiencies of the gas boiler and coal boiler are 2.32, 90%, and 40% [38], respectively. The duration of the heating season in Beijing was determined to be 120 days and ten hours per day. According to Equations (8) and (9), the derived carbon emissions values of ASHP, gas boiler, and coal boiler during the entire heating season are 1406.1 $kgCO_2$, 1196.2 $kgCO_2$, and 4310.4 $kgCO_2$, respectively. Correspondingly, the carbon emissions values per unit area are 14.6 $kgCO_2/m^2$, 12.5 $kgCO_2/m^2$, and 44.9 $kgCO_2/m^2$, respectively.

Therefore, to enhance environment quality and respond to the carbon peak target, the heating type driven by the coal boiler has been gradually phased out, while heating driven by ASHP or gas boiler are in accordance with real conditions. For example, ASHP has been widely adopted due to its easy installation, high energy savings, and low carbon emissions in Beijing. Meanwhile, in Hebei, heating is mostly supplied by heat from gas on account of its cost-effectiveness and significant reduction in carbon emissions.

4.6. Limitations and Future Research

The limitations and future research work of this study are as follows:

The gray box thermal model utilized is specifically applied to selected rural residential buildings in our paper. However, for other buildings, the selection of RC model in this paper may lead to errors due to variations in building shape, window-wall ratio, and plane layout. Future research aims to explore appropriate models for the values of R and C by considering buildings with diverse structural characteristics, ultimately summarizing RC models suitable for different building structural and usage characteristics.

In the modeling process, numerous assumptions have been made, and several crucial considerations have been omitted by this study, which may impact the resulting changes. These factors encompass the building's age, the heat storage function of furniture and equipment, and the duration of occupants' activity. These factors should be taken into account in future refinement of the modeling process to achieve the desired level of accuracy.

5. Conclusions

This paper presents an equivalent 3R2C model to predict dynamic heating load and total carbon emissions during the entire heating season. The data monitored from an ASHP heating system in a rural residence in Beijing are used to train R and C, and validation is conducted with different meteorological conditions. The main conclusions are as follows:

(1) With increasing training time, better following quality between predicted indoor air temperature and actual measured temperature is obtained. When the training time increases to eight hours from one hour, the correlation coefficient increases to 95.45% from 63.15%. The minimum *MAE*, *MAPE*, and *RMSE* values are obtained by training of eight hours, which are 9.79%, 0.55%, and 12.26%, respectively.

(2) Validation test results of the other four different periods show that regardless of the weather condition, the correlation coefficient is beyond 96%, and the covariance is more than 20%. Under severe cold, cold, cool, and mild weather, *RMSE* values are 17.91%, 19.71%, 23.32%, and 12.53%, respectively.

(3) A method of estimating carbon emissions and energy consumption is proposed based on the established RC model. The energy consumption index per unit area under standard weather conditions in Beijing can be derived, and it is 46.77 W/m^2. Meanwhile, the carbon emissions per unit area values of ASHP, gas boiler, and coal

boiler during the entire heating season are 14.6 $kgCO_2/m^2$, 12.5 $kgCO_2/m^2$, and 44.9 $kgCO_2/m^2$, respectively.

Author Contributions: Conceptualization, L.K.; Methodology, L.K.; Software, H.L.; Formal analysis, H.L.; Investigation, J.W.; Resources, Z.W.; Data curation, J.W. and D.S.; Writing—original draft, L.K.; Writing—review & editing, L.K. and Y.Y.; Project administration, Z.W. All authors have read and agreed to the published version of the manuscript.

Funding: This work was supported by the Opening Funds of State Key Laboratory of Building Safety and Built Environment (grant number: BSBE-EET2021-01).

Data Availability Statement: Data are contained within the article.

Conflicts of Interest: The authors declare no conflict of interest.

Nomenclature

A	building heating area
C	Thermal capacitance
CE	total carbon emissions
CE_0	carbon emissions per unit aera
CEF	carbon emission factor
COP	coefficient of performance
m	mass flow rate of water
P	power consumption
Q	nominal heating capacity
R	thermal resistance
T	temperature
ρ	density
c_p	specific heat
Subscripts and Superscripts	
in	indoor air
inf	infiltration
m	internal thermal mass
oe	opaque envelope
out	outdoor air
r	return water
s	supply water
Abbreviations	
ASHP	air source heat pump
BIM	building information modeling
GA	genetic algorithm
MAE	mean absolute error
$MAPE$	mean absolute percentage error
RC	model resistance-capacitance model
$RMSE$	root-mean square error

References

1. Norouziasl, S.; Jafari, A. Identifying the most influential parameters in predicting lighting energy consumption in office buildings using data-driven method. *J. Build. Eng.* **2023**, *72*, 106590. [CrossRef]
2. Kang, L.; Wang, J.; Yuan, X.; Cao, Z.; Yang, Y.; Deng, S.; Zhao, J.; Wang, Y. Research on energy management of integrated energy system coupled with organic Rankine cycle and power to gas. *Energy Convers. Manag.* **2023**, *287*, 117117. [CrossRef]
3. Liang, X.; Chen, S.; Zhu, X.; Jin, X.; Du, Z. Domain knowledge decomposition of building energy consumption and a hybrid data-driven model for 24-h ahead predictions. *Appl. Energy* **2023**, *344*, 121244. [CrossRef]
4. Tadeu, S.; Rodrigues, C.; Marques, P.; Freire, F. Eco-efficiency to support selection of energy conservation measures for buildings: A life-cycle approach. *J. Build. Eng.* **2022**, *61*, 105142. [CrossRef]
5. Luo, X.; Ren, M.; Zhao, J.; Wang, Z.; Ge, J.; Gao, W. Study on the life-cycle carbon emission and energy-efficiency management of the large-scale public buildings in Hangzhou, China. *J. Clean. Prod.* **2022**, *367*, 132930. [CrossRef]
6. Xu, Y.; Yan, C.; Wang, G.; Shi, J.; Sheng, K.; Li, J.; Jiang, Y. Optimization research on energy-saving and life-cycle decarbonization retrofitting of existing school buildings: A case study of a school in Nanjing. *Sol. Energy* **2023**, *254*, 54–66. [CrossRef]

7. Oscar, O.; Castells, F.; Sonnemann, G. Life cycle assessment of two dwellings: One in Spain, a developed country, and one in Colombia, a country under development. *Sci. Total Environ.* **2010**, *408*, 2435–2443.
8. Biswas, W.; Wahidul, K. Carbon footprint and embodied energy consumption assessment of building construction works in Western Australia. *Int. J. Sustain. Built Environ.* **2014**, *3*, 179–186. [CrossRef]
9. Luo, X.; Oyedele, L. A data-driven life-cycle optimisation approach for building retrofitting: A comprehensive assessment on economy, energy and environment. *J. Build. Eng.* **2021**, *43*, 102934. [CrossRef]
10. Kneifel, J. Life-cycle carbon and cost analysis of energy efficiency measures in new commercial buildings. *Energy Build.* **2010**, *42*, 333–340. [CrossRef]
11. Rabani, M.; Madessa, H.B.; Ljungström, M.; Aamodt, L.; Løvvold, S.; Nord, N. Life cycle analysis of GHG emissions from the building retrofitting: The case of a Norwegian office building. *Build. Environ.* **2021**, *204*, 108159. [CrossRef]
12. Zhang, Y.; Jiang, X.; Cui, C.; Skitmore, M. BIM-based approach for the integrated assessment of life cycle carbon emission intensity and life cycle costs. *Build. Environ.* **2022**, *226*, 109691. [CrossRef]
13. Peng, C. Calculation of a building's life cycle carbon emissions based on Ecotect and building information modeling. *J. Clean. Prod.* **2016**, *112*, 453–465. [CrossRef]
14. Liang, Y.; Pan, Y.; Yuan, X.; Yang, Y.; Fu, L.; Li, J.; Sun, T.; Huang, Z.; Kosonen, R. Assessment of operational carbon emission reduction of energy conservation measures for commercial buildings: Model development. *Energy Build.* **2022**, *268*, 112189. [CrossRef]
15. Zhang, C.; Luo, H. Research on carbon emission peak prediction and path of China's public buildings: Scenario analysis based on LEAP model. *Energy Build.* **2023**, *289*, 113053. [CrossRef]
16. Verbeeck, G.; Hens, H. Life cycle inventory of buildings: A calculation method. *Build. Environ.* **2010**, *45*, 1037–1041. [CrossRef]
17. Shao, L.; Chen, G.; Chen, Z.; Guo, S.; Han, M.; Zhang, B.; Hayat, T.; Alsaedi, A.; Ahmad, B. Systems accounting for energy consumption and carbon emission by building. *Commun. Nonlinear Sci. Numer. Simul.* **2014**, *19*, 1859–1873. [CrossRef]
18. Iddon, C.; Firth, S. Embodied and operational energy for new-build housing: A case study of construction methods in the UK. *Energy Build.* **2013**, *67*, 479–488. [CrossRef]
19. Zhang, Z.; Wang, B. Research on the life-cycle CO_2 emission of China's construction sector. *Energy Build.* **2016**, *112*, 244–255. [CrossRef]
20. Zhu, W.; Feng, W.; Li, X.; Zhang, Z. Analysis of the embodied carbon dioxide in the building sector: A case of China. *J. Clean. Prod.* **2020**, *269*, 122438. [CrossRef]
21. Gan, V.J.; Cheng, J.C.; Lo, I.M.; Chan, C. Developing a CO_2-e accounting method for quantification and analysis of embodied carbon in high-rise buildings. *J. Clean. Prod.* **2017**, *141*, 825–836. [CrossRef]
22. Mao, X.; Wang, L.; Li, J.; Quan, X.; Wu, T. Comparison of regression models for estimation of carbon emissions during building's lifecycle using designing factors: A case study of residential buildings in Tianjin, China. *Energy Build.* **2019**, *204*, 109519.
23. Zhang, N.; Luo, Z.; Liu, Y.; Feng, W.; Zhou, N.; Yang, L. Towards low-carbon cities through building-stock-level carbon emission analysis: A calculating and mapping method. *Sustain. Cities Soc.* **2022**, *78*, 103633. [CrossRef]
24. Acquaye, A.; Duffy, A.; Basu, B. Embodied emissions abatement—A policy assessment using stochastic analysis. *Energy Policy* **2011**, *39*, 429–441. [CrossRef]
25. Röck, M.; Baldereschi, E.; Verellen, E.; Passer, A.; Sala, S.; Allacker, K. Environmental modelling of building stocks—An integrated review of life cycle-based assessment models to support EU policy making. *Renew. Sustain. Energy Rev.* **2021**, *151*, 111550. [CrossRef]
26. Lomas, K. Carbon reduction in existing buildings: A transdisciplinary approach. *Build. Res. Inf.* **2010**, *38*, 1–11. [CrossRef]
27. Rogers, J.; Cooper, S.; O'Grady, Á.; McManus, M.; Howard, H.; Hammond, G. The 20% house—An integrated assessment of options for reducing net carbon emissions from existing UK houses. *Appl. Energy* **2015**, *138*, 108–120. [CrossRef]
28. Airaksinen, M.; Matilainen, P. A Carbon Footprint of an Office Building. *Energies* **2011**, *4*, 1197–1210. [CrossRef]
29. Ye, H.; Wang, K.; Zhao, X.; Chen, F.; Li, X.; Pan, L. Relationship between construction characteristics and carbon emissions from urban household operational energy usage. *Energy Build.* **2011**, *43*, 147–152. [CrossRef]
30. *JGJ/T 132-2009*; Standard for Energy Efficiency Test of Residential Building. China Architecture and Building Press: Beijing, China, 2010.
31. Wang, J.; Jiang, Y.; Tang, C.Y.; Song, L. Development and validation of a second-order thermal network model for residential buildings. *Appl. Energy* **2022**, *306*, 118124. [CrossRef]
32. Harb, H.; Boyanov, N.; Hernandez, L.; Streblow, R.; Müller, D. Development and validation of grey-box models for forecasting the thermal response of occupied buildings. *Energy Build.* **2016**, *117*, 199–207. [CrossRef]
33. Danza, L.; Belussi, L.; Meroni, I.; Salamone, F.; Floreani, F.; Piccinini, A.; Dabusti, A. A simplified thermal model to control the energy fluxes and to improve the performance of buildings. *Energy Procedia* **2016**, *101*, 97–104. [CrossRef]
34. Ivanica, R.; Risse, M.; Weber-Blaschke, G.; Richter, K. Development of a life cycle inventory database and life cycle impact assessment of the building demolition stage: A case study in Germany. *J. Clean. Prod.* **2023**, *338*, 130631. [CrossRef]
35. Raid, A.; Marah, A.; Jochen, A. A data-driven predictive maintenance model for hospital HVAC system with machine learning. *Build. Res. Inf.* **2023**, *51*, 2206989.
36. Xu, Z.; Zhao, W.; Shao, S.; Wang, Z.; Xu, W.; Li, H.; Wang, Y.; Wang, W.; Yang, Q.; Xu, C. Analysis on key influence factors of air source heat pumps with field monitored data in Beijing. *Sustain. Energy Technol. Assess.* **2021**, *48*, 101642. [CrossRef]

37. *DB11/T 1784-2020*; Requirements for Carbon Dioxide Emission Accounting and Reporting Heat Production and Supply Enterprises. China Standards Publishing House: Beijing, China, 2020.
38. Yang, Y. *Heating Carbon Emission and System Improvement for Rural Building of Beijing*; China Academy of Building Research: Beijing, China, 2019.